Article

Design of Potent mRNA Decapping Scavenger Enzyme (DcpS) Inhibitors with Improved Physicochemical Properties to Investigate the Mechanism of Therapeutic Benefit in Spinal Muscular Atrophy (SMA)

Ariamala Gopalsamy, Arjun Narayanan, Shenping Liu, Mihir D. Parikh, Robert E. Kyne, Jr., Olugbeminiyi O Fadeyi, Michael A Tones, Jonathan J. Cherry, Joseph F. Nabhan, Gregory LaRosa, Donna N Petersen, Carol A. Menard, Timothy L Foley, Stephen Noell, Yong Ren, Paula M. Loria, Jodi Maglich-Goodwin, Haojing Rong, and Lyn H. Jones

Just Accepted

Design of Potent mRNA Decapping Scavenger Enzyme (DcpS) Inhibitors with Improved Physicochemical Properties to Investigate the Mechanism of Therapeutic Benefit in Spinal Muscular Atrophy (SMA)

Ariamala Gopalsamy,[§]* Arjun Narayanan,[§] Shenping Liu,[⊥] Mihir D. Parikh,[⊥] Robert E. Kyne Jr.,[⊥] Olugbeminiyi Fadeyi,[⊥] Michael A. Tones[‡], Jonathan J. Cherry,[‡] Joseph F. Nabhan,[‡] Gregory LaRosa,[‡] Donna N. Petersen,[†] Carol Menard,[†] Timothy L. Foley,[†] Stephen Noell,[†] Yong Ren,[†] Paula M. Loria,[†] Jodi Maglich-Goodwin,[§] Haojing Rong,[#] Lyn H. Jones[§]

[§]Medicine Design and [‡]Rare Disease Research Unit, [#]Pharmacokinetics and Drug Metabolism, Pfizer, 610 Main Street, Cambridge, Massachusetts 02139, USA

[⊥]Medicine Design and [†]Primary Pharmacology Group, Pfizer, Eastern Point Road, Groton, Connecticut 06340, USA

1
2
3
4
5
6
7
8
9
10
11
12
13
14
15
16
17
18
19
20
21
22
23
24
25
26
27
28
29
30
31
32
33
34
35
36
37
38
39
40
41
42
43
44
45
46
47
48
49
50
51
52
53
54
55
56
57
58
59
60

ABSTRACT

The C-5 substituted 2,4-diaminoquinazoline RG3039 (compound **1**), a member of a chemical series that was identified and optimized using an SMN2 promoter screen, prolongs survival and improves motor function in a mouse model of spinal muscular atrophy (SMA). It is a potent inhibitor of the mRNA Decapping Scavenger Enzyme (DcpS), but the mechanism whereby DcpS inhibition leads to therapeutic benefit is unclear. Compound **1** is a dibasic lipophilic molecule that is predicted to accumulate in lysosomes. To understand if the *in-vivo* efficacy is due to DcpS inhibition or other effects resulting from the physicochemical properties of the chemotype, we undertook structure based molecular design to identify DcpS inhibitors with improved physicochemical properties. Herein we describe the design, synthesis, *in-vitro* pharmacological characterization of these DcpS inhibitors along with the *in-vivo* mouse CNS PK profile of PF-DcpSi (compound **24**), one of the analogs found to be efficacious in SMA mouse model.

KEYWORDS – SMA, Spinal Muscular Atrophy, DcpS, mRNA Decapping Scavenger Enzyme, DcpS inhibitor, LipE, Lipophilic Efficiency

INTRODUCTION

Spinal muscular atrophy (SMA) is an autosomal recessive, inherited neurodegenerative disease and a leading genetic cause of infant death. It is characterized by loss of alpha-motor neurons in the spinal cord leading to progressive atrophy and weakness of limb and trunk muscles.[1, 2] There is currently no cure for SMA.[3] Humans carry two Survival Motor Neuron (SMN) genes: *SMN1* and *SMN2*. SMA is caused by deficiency of the SMN protein resulting from homozygous deletion of *SMN1*, partly compensated for by the presence of the paralogous gene *SMN2*. While both SMN1 and SMN2 encode an identical protein, full length protein production occurs at much lower efficiency from *SMN2* than from *SMN1* due to the exclusion of Exon-7 from the majority of *SMN2* transcripts leading to their degradation. An attractive potential therapeutic approach is to increase the *SMN2* promoter activity.[4] This approach was employed by Jarecki et al. to identify C5-substituted 2,4-diaminoquinazolines[5] from a high throughput reporter gene assay using the SMN2 promoter to drive β-lactamase activity.[6] Further follow-up was carried out using protein microarray scanning with a radiolabelled C5-substituted 2,4-diaminoquinazoline probe that identified DcpS as a single binding protein. We recently reported[7] the results of a related protein microarray and affinity capture technique that confirmed the exquisite selectivity of the 2,4-diaminoquinazoline template. DcpS thus became a potential novel therapeutic target for modulating gene expression.[8]

Eukaryotic mRNA turnover pathway begins with deadenylation followed by decapping and 5'→3' exonucleolytic degradation. This process results in accumulation of residual N-7 guanine cap from the degraded mRNA. The human decapping scavenger enzyme (DcpS) catalyzes residual cap hydrolysis following mRNA degradation and prevents accumulation of intermediates that might interfere with translation and normal processing of mRNAs.[9-12] By

restoring this essential function, DcpS protects the cell from the potential toxic accumulation of capped mRNA fragments and plays a regulatory role. DcpS belongs to the HIT family of pyrophosphatases[13] and its structure bound to either m7GpppG or m7GpppA reveals an asymmetric dimer with a domain-swapped amino terminus.[14] DcpS is a dimeric protein with two distinct cap binding pockets. It exists as a symmetrical dimer with open conformation in the ligand-free state and adopts an asymmetric conformation when bound to ligand, with one site open and other site closed. C5-substituted 2,4-diaminoquinazolines identified from the reporter screen potently inhibit DcpS and were found to occupy the cap binding pocket when co-crystallized with the enzyme. While its role in mRNA turnover is well established, DcpS is an unprecedented drug discovery target.

RG3039 (compound **1**), one of the advanced C5-substituted 2,4-diaminoquinazolines to enter Phase 1 clinical development, is effective in prolonging the survival of SMA mice after oral administration.[15, 16] We appreciated that **1** is a lipophilic dibasic compound – the calculated LogP of 5.3 and measured pKas of 8.1 and 7.8 confirmed this assertion. Compounds with these physicochemical properties have the propensity to accumulate in tissues as the result of partitioning into membranes and entrapment within the lysosomal compartment by virtue of protonation in its acidic environment.[17] So-called lysosomotropic agents have been reported to provide neuroprotection in a model of neurodegeneration involving activation of apoptosis.[18] Additionally, lysosomotropism contributes to autophagy perturbation,[19] and autophagic dysregulation is a feature of SMA.[20, 21] To understand if the *in-vivo* efficacy of **1** is due to a DcpS-dependent mechanism or due to the physicochemical properties of the chemotype, we sought to develop potent DcpS inhibitors devoid of lysosomotropism, with adequate pharmacokinetics (and possessing the requisite CNS free drug levels) to test in an *in-vivo* SMA

mouse model. Herein, we describe the structure-based design of potent DcpS inhibitors with improved physicochemical properties and report that therapeutic benefit in SMA is consistent with a DcpS-related mechanism. We also describe the creation of a 2,4-diaminoquinoline derivative that is closely related in structure to our lead equity, but which is DcpS inactive and therefore serves as a useful negative control chemical probe of DcpS biology.

RESULT AND DISCUSSIONS

Chemistry

Compounds **1-8** (Table 1) were synthesized as disclosed previously for the synthesis of **1**, as shown in Scheme I. 2,4-diamonquinazolines functionalized at the C5 position were prepared by reaction of Boc protected piperidine alcohol **30** with 2,6-difluorobenzonitrile **31.** Resulting 2-fluoro-6-arylalkoxybenzonitrile **32** was cyclized to give intermediate **33** by heating with guanidine carbonate in N,N-dimethylacetamide at high temperature. The removal of the protecting group under standard acidic conditions to generate intermediate **34**, followed by alkylation with various substituted benzyl bromides afforded corresponding 5-substituted 2,4-diaminoquinazolines **1-8** (Scheme 1). The aliphatic ether linked racemate compound **37** was obtained in two steps from intermediate **31,** F displacement followed by cyclization. The racemate **37** was separated by chiral SFC to give single enantiomers **15** and **16** (Scheme 2).

The reverse ether analog **25** was synthesized from 2-fluoro-6-methylbenzonitrile **38.** Radical bromination of **38** afforded 2-(bromomethyl)-6-fluorobenzonitrile **39**. Displacement of substituted benzyl bromide with **40** in presence of potassium carbonate afforded **41**, which was subsequently cyclized using guanidine carbonate to yield **25**. The compound **25** was further converted into crystalline hydrochloride salt **25a** (Scheme 3). The synthesis of C5, C7

disubstituted 2,4-diamonquinazolines is shown in Scheme 4. 2,6-difluoro-4-methylbenzonitrile **43** was the common intermediate for C7 substituted ring systems, which was synthesized by Suzuki coupling of **42**. Displacement with **30** followed by cyclization and deprotection provided intermediate **46**, which was alkylated with 2-(bromomethyl)-1,3-dichlorobenzene **47** to afford 7-methyl-5-substituted 2,4-diaminoquinazoline **26.**

The synthesis of C7 substituted reverse ether analog **28** is shown in Scheme 5. Bromination of aniline **48** afforded **49**. The amino group was converted to cyano using Sandmeyer reaction 5**0**. Formylation using iPrMgCl at low temperature gave **51**, which was reduced under mild conditions to give primary alcohol **52** without any lactone formation through intramolecular cyclization. The alkyl halide **53** was displaced with phenol **54** and then cyclized to afford reverse ether analog **28**.

Cellular Accumulation

The physicochemistry of DcpS inhibitors such as **1** is suggestive of lysosomal accumulation which may impact autophagic phenotypes in SMA mouse models. In order to investigate the cellular accumulation of the C5-substituted 2,4-diaminoquinazolines, an evaluation of compound **1** and close analogs (compound **2** and **3**) (Fig 1) in HEK293T cells and lymphoblasts was carried out in the presence and absence of either concanamycin A and bafilomycin. These compounds block lysosomal acidification through selective inhibition of the vacuolar type ATPase[22] that establishes the low pH environment of the lysosome. Chloroquine, a well-established lysosomotrope, was included in these experiments as a positive control. As expected, chloroquine accumulation by cells was inhibited by >98% by the presence of either bafilomycin or concanamycin A. Similarly, significant accumulation of **1** and the other lipophilic dibasic C5-substituted diaminoquinazolines compound **2** and compound **3** was also observed and

was also largely inhibited by either of the two inhibitors of lysosomal acidification (Fig 2). This observation prompted us to investigate the requirement of the dibasic lipophilic moieties for DcpS inhibition, to eventually avoid potential issues arising from lysosomotropism-related effects. The design and synthesis of analogs with improved pharmaceutical properties along with further biological profiling of both classes of DcpS inhibitors is described below.

Structure Based Design of DcpS Inhibitors

The structure-activity relationship generated for C5-substituted 2,4-diaminoquinazolines in the earlier iteration that led to the identification of compound **1** utilized an SMN promoter assay and lacked a targeted assay such as DcpS inhibition assay for inhibitor optimization. In the absence of target information, structure-based ligand design was not utilized at that time. Currently, the 2,4-diaminoquinazoline pharmacophore that mimics the 7-methylguanine mRNA cap structure is the only reported chemotype known to block cap binding to DcpS. The co-crystal structure of compound **2** (PDB ID code: 3BL7) shown in Fig 3 (Left) explains the excellent complementarity exhibited by this scaffold. The template 2,4-diaminoquinazoline is critical for activity since in its protonated state it invokes a network of hydrogen bonds. Glu-185 forms a strong bidentate hydrogen bond to the N1 and C2-NH$_2$, which additionally forms a strong hydrogen bond to the backbone carbonyl of Pro204. The flat bicyclic quinazoline scaffold engages in productive $\pi-\pi$ stacking with Trp-175, CH-π interaction with Leu-206, and an edge-to-face interaction with the π system of Tyr-113, leading to excellent packing of the quinazoline ring. From steric considerations, the C5 position of the quinazoline provides an appropriate vector to extend, mimicking cap binding in the DcpS active site. However, the region occupied by the C-5 substituent (2,6-dichlorobenzyl substituted piperidinemethyl in **1**) is an elongated pocket (Fig 3 - Right). As seen from the structure of cap-bound DcpS, this pocket

accommodates the phosphate groups and the base. This region of the pocket therefore seemed amenable to investigate further structure-activity relationships, and hence we targeted this region to optimize the physicochemical properties of compound **1**.

From the structure activity data published for the SMN2 promoter driven reporter assay, it appeared that the lipophilic achiral piperidine substituent in **1** resulted from the desire to overcome cellular toxicity that was attributed to dihydrofolate reductase (DHFR) enzyme inhibition as an off-target for the quinazoline chemotype. Based on the reported data, lipophilic halogenated benzyl groups were pursued to improve potency in the SMN2 promoter assay (Table 1). We initiated profiling of a cohort of compounds which were active in the SMN2 promoter assay in the DcpS (human DcpS) enzyme assay. Compounds were indeed very potent in this biochemical assay.[23, 24] However, successful medicinal chemistry programs often do not focus exclusively on potency, but rather balance a myriad of features that include metabolic stability, solubility and off-target selectivity for a favorable *in vivo* outcome. A more useful parameter in the design process is lipophilic efficiency,[25] which normalizes the potency achieved with the lipophilicity of the molecule (LipE = pIC_{50} – LogP) thus serving as a useful descriptor of drug-like characteristics. High lipophilicity can drive poor metabolic stability, solubility and polypharmacology, hence a higher LipE is preferable. Hence, towards our goal of reducing lipophilicity, while retaining adequate DcpS potency, we generated LipE plots (Figure 4) of the lipophilic piperidine analogs along with some non-piperidine analogs using DcpS inhibitory activity. As seen from the LipE plot and Table 1, the lipophilic efficiency of **1** (LipE: 4.9) and the close-in analogs were not inferior to the simple unsubstituted 2,4-diaminoquinazoline template (compound **9**: LipE: 5.8) and the minimally substituted 5-methoxy-2,4-diaminoquinazoline (Compound **10**: LipE: 6.6).

Simple aliphatic/alicyclic groups at the C5-position using synthetically expedient ether linkages, as represented by analogs **14-18**, resulted in moderate DcpS activity compared to the piperidine analogs shown in Table 2. However, these analogs exhibited superior lipophilic efficiency as shown in Table 2 and Fig 4. From the ligand-bound crystal structure of DcpS, the C-5 substituents are placed in a hydrophobic environment and an aromatic ring seems to provide the best complementarity. Based on this analysis, unsubstituted and halogen-substituted aromatic ethers (compounds **11-13**) were evaluated for DcpS inhibitory activity and were found to be more active than the aliphatic analogs. However, this modification resulted in increased lipophilicity, thus compromising the lipophilic efficiency. The corresponding reverse ether analogs provided a slight boost in potency with an added advantage of reduced cLogP. The replacement of an aromatic chloride with a nitrile often improves LipE,[26] hence a nitrile group was introduced in the aryl ether substituent to yield compound **24**. Additionally, the replacement of the nitrile with a bioisosteric[27] pyridine derivative as in compound **25**, retained the improved LipE. The reverse ether analogs had an added advantage with respect to DHFR selectivity as shown in Table 2.

Physicochemical Properties

As predicted, analogs with less lipophilic C5-substituents showed higher metabolic stability. These compounds also showed potential for good brain penetration as determined by the MDR BA/AB ratio of <2.5 and good aqueous solubility. *In-vitro* ADME and physicochemical profiling of selected non-lipophilic compounds in comparison to the original lipophilic series (exemplified by derivative **1)** is shown in Fig 5. Table 3 shows the physicochemical properties improvement of representative examples **24** and **25** in comparison to compound **1**.

Having identified potent DcpS inhibitors with improved physicochemical properties, a representative analog Compound **25**, was evaluated for cellular accumulation in the presence and absence of either concanamycin A or bafilomycin. In marked contrast to **1** and close analogs, compound **25** showed dramatically reduced cellular accumulation. As a result, the concentration of compound **25** in cells was too low to reliably determine the effect of bafilomycin or concanamycin A (Fig 6).

Pharmacokinetics (PK)

Towards the goal of understanding if *in-vivo* efficacy is due to a DcpS-dependent mechanism and not the effect of the physicochemical properties of the chemotype, one of the optimized analogs, compound **24** was selected for *in-vivo* PK investigation. *In-vivo* PK evaluation of compound **24** was carried out in WT mice (FVB/N) to understand the free compound exposure in plasma, brain and CSF (Table 4). Free drug levels in brain were ~2.5 fold lower than that unbound in plasma, indicating minimal brain impairment. The PK data indicated that free drug levels in brain were above the required coverage based on an estimated IC_{90} concentration for DcpS inhibition. With adequate CNS exposure achieved compound **24** was evaluated in the 2B/- SMA mouse model and found to be effective in ameliorating the disease phenotype in these mice. This result is consistent with DcpS inhibition being the mechanism of action underlying therapeutic benefit of the C5-substituted 2,4-diaminoquinazolines in SMA. These data and a comprehensive study of the biological effects of DcpS inhibitors in cells *in-vitro* and *in-vivo* are the subject of another report.[28]

Design of matched inactive analogs of DcpS inhibition

Towards our ultimate goal of understanding if the efficacy observed in SMA mouse models by administering **1** is due to DcpS inhibition or due to the physicochemical and/or

general structural characteristics of the chemotype, we were in need of structurally-similar but DcpS inactive 2,4-diaminoquinazolines as tool compounds. While scouting for inactive tool compounds is not a common strategy in a drug discovery paradigm, such tools are an important part of successful target validation[29] and have the potential to unearth unprecedented molecular pathways. Closely matched active/inactive pairs of compounds were generated using our structural knowledge of the interaction of the C-5 substituted 2,4-diaminoquinazolines with the DcpS. As seen in Fig 8 (left panel), the quinazoline template occupies the binding pocket making a favorable edge to face interaction with Tyr113 and any substitution from the 7-position of the aromatic ring will not be accommodated (Fig 8, right panel). This prompted us to make use of this spatial constraint to design 7-substituted 2,4-diamino analogs as close-in matched inactive analogs.

A subset of potent DcpS inhibitors (compounds **1, 2, 17, 24**) from the C5-substitued 2,4-diaminoquinazolines were chosen to explore substituent effects in the 7-position. The methyl substituent was chosen to maintain the electronics of the diaminoquinazoline ring while providing a potentially significant steric clash with the protein. As shown in Table-5 all the 7-methyl analogs (compound **26-29**) were considerably less active compared to the 7-H DcpS inhibitors. As anticipated, irrespective of the length or nature of the C-5 substituents, 7-Me substituted 2,4-diaminoquinazolines possessed the desired loss of Dcps activity. These tool compounds serve as useful probes in a DcpS toolkit for further target validation and were extensively used in further *in-vitro* studies.[28]

CONCLUSION

Compound **1** is a dibasic lipophilic C-5-disubstituted 2,4-diaminoquinazoline analog that prolongs survival and function in SMA mouse models. While the compound is a potent DcpS

inhibitor, in the absence of a direct link to the mechanistic role of DcpS inhibition for efficacy, lysosomotropism was considered as a possible contributor to *in-vivo* efficacy. To shed more light to this, we employed rational structure-based design of potent DcpS inhibitors with improved physicochemical properties with adequate CNS exposure to evaluate *in-vivo*. Compound **24** was found to be efficacious in an SMA mouse model by prolonging survival and improving function thereby ruling out lysosomotropism as the mechanism of efficacy. Compound **24** (referred to now as PF-DcpSi) and related analogs with good physicochemical properties, along with the matched pair of inactive analogs, provide key starting points for understanding DcpS as a drug discovery target for spinal muscular atrophy.

EXPERIMENTAL SECTION

General information

Chemicals were typically obtained from Sigma-Aldrich or Alfa Aesar and used as received, unless noted otherwise. Solvents were commercial anhydrous grade, used as received. Unless otherwise stated, reactions were run under a positive pressure of nitrogen at ambient temperature. "Flash chromatography" refers to normal phase chromatography using a medium pressure Biotage or ISCO system employing commercial pre-packed silica gel columns. Analytical thin layer chromatography (TLC) was performed on 60 F254 glass plates pre-coated with a 0.25-mm thickness of silica gel purchased from EMD chemical Inc. TLC plates were visualized with UV light.

^{1}H , ^{13}C (^{1}H decoupled), and ^{19}F (^{1}H decoupled) nuclear magnetic resonance (NMR) spectra were recorded on a Bruker or Varian spectrometer operating at 400, 101 and 376 MHz, respectively, or a Bruker 500 MHz spectrometer operating at 500, 126 and 470 MHz, respectively. Chemical shifts reported in parts per million (δ) relative to CDCl3 (^{1}H NMR,

7.26 ppm; ^{13}C NMR, 77.00 ppm), DMSO-*d*6 (^{1}H NMR, 2.50 ppm; ^{13}C NMR, 39.52 ppm), CD$_3$OD (^{1}H NMR, 3.31 ppm; ^{13}C NMR; 49.00 ppm), D$_2$O (^{1}H NMR 4.79 ppm), CD$_2$Cl$_2$ (^{13}C NMR 54.00 ppm) The following abbreviations are used for peak multiplicities: s = singlet, d = doublet, t = triplet, m = multiplet, br = broadened, dd = doublet of doublets, dt = doublet of triplets. Low resolution mass spectroscopy was carried out using 1) liquid chromatography−mass spectrometry (LCMS) on a Waters Acquity UPLC instrument using atmospheric pressure chemical ionization (APCI) or electrospray ionization (ESI), or 2) by gas chromatography-mass spectroscopy (GCMS) on an Agilent 5975 series instrument with electron ionization (EI). High resolution mass measurements were carried out on an Agilent TOF 6200 series instrument with ESI. The purity of final compounds as measured by HPLC was at least above 95%.

All procedures involving animals were conducted as per the study protocols approved by Pfizer or other Institutional Animal Care and Use Committee and, in compliance with applicable institutional guidelines, state & national regulations and the Guide for Care and Use of Laboratory Animals.

Compounds **1**- **8** were prepared as described in Reference 5.

(S)-5-((1-Methoxypropan-2-yl)oxy)quinazoline-2,4-diamine (15) and (R)-5-((1-Methoxypropan-2-yl)oxy)quinazoline-2,4-diamine (16). Compound **37** (140 mg) was separated by chiral SFC (ChiralPak AD (250x30mm, 20 μm); 40% EtOH (0.05% NH$_3$ in H$_2$O); 80 mL/min) to give two peaks arbitrarily assigned: **15** (peak 1, RT = 7.958 min, 39 mg, 28 %) as a yellow solid: LC/MS (ESI) m/z 249.0 [M+H]$^+$; ^{1}H NMR (400 MHz, METHANOL-d$_4$) δ 7.34 (t, *J*=8.20 Hz, 1H), 6.78 (d, *J*=7.80 Hz, 1H), 6.60 (d, *J*=8.20 Hz, 1H), 4.63-4.74 (m, 1H), 3.40-3.69 (m, 2H), 3.32 (s, 2H), 1.31 (d, *J*=6.24 Hz, 2H); ^{13}C NMR (101 MHz, METHANOL-d$_4$) δ

163.0, 160.2, 156.1, 153.3, 133.3, 115.7, 104.4, 102.2, 74.8, 74.3, 58.1, 15.1; HRMS m/z calcd

for $C_{12}H_{16}N_4O_2$ [M+H]$^+$: 249.1346. Found: 249.1354 and **16** (peak 2, RT = 9.19 min, 39 mg,

28%) as a white solid: LC/MS (ESI) m/z 248.9 [M+H]$^+$; ^{1}H NMR (400 MHz, METHANOL-d$_4$)

δ 7.35 (t, *J*=8.20 Hz, 1H), 6.78 (d, *J*=8.20 Hz, 1H), 6.60 (d, *J*=8.20 Hz, 1H), 4.63-4.74 (m, 1H),

3.43-3.62 (m, 2H), 3.32 (s, 3H), 1.30 (d, *J*=6.24 Hz, 3H); ^{13}C NMR (101 MHz, METHANOL-d$_4$)

δ 163.0, 160.1, 156.1, 153.2, 133.3, 115.6, 104.5, 102.2, 74.8, 74.3, 58.1, 15.1; HRMS m/z calcd

for $C_{12}H_{16}N_4O_2$ [M+H]$^+$: 249.1346. Found: 249.1353.

5-(((Tetrahydro-2H-pyran-4-yl)oxy)methyl)quinazoline-2,4-diamine   (18).   The

procedure used to prepare compound **25** was used to prepare compound **18**; using commercially

available tetrahydro-2H-pyran-4-ol and 2-(bromomethyl)-6-fluorobenzonitrile **(39)** as reagents in

the initial nucleophilic displacement step followed by cyclization: ^{1}H NMR (400 MHz, DMSO-

d$_6$) δ 7.37-7.47 (m, 1H), 7.30 (br. s., 2H), 7.23 (d, *J*=8.59 Hz, 1H), 7.03 (d, *J*=6.63 Hz, 1H), 6.01

(br. s., 2H), 4.78 (s, 2H), 3.77-3.86 (m, 2H), 3.74 (td, *J*=4.59, 8.78 Hz, 1H), 3.37-3.42 (m, 2H),

1.90-1.93 (m, 2H), 1.37-1.57 (m, 2H); ^{13}C NMR (101 MHz, DMSO-d$_6$) δ 163.1, 160.6, 155.4,

134.0, 132.0, 126.4, 124.8, 111.1, 73.2, 69.5, 65.2, 32.5; HRMS (ESI) m/z: calculated for

$C_{14}H_{18}N_4O_2$ [M + H]$^+$ 275.1503; observed 275.1509.

3-((2,4-Diaminoquinazolin-5-yl)methoxy)-5-fluorobenzonitrile (24). Compound **24**

was prepared similarly to **25** using commercially available 3-fluoro-5-hydroxybenzonitrile and 2-

(bromomethyl)-6-fluorobenzonitrile **(39)** as reagents in the nucleophilic displacement step

followed by cyclization, compound was purified by reverse phase HPLC using a gradient of

water and acetonitrile (95:5 to 5:95) to give **24** (7 mg, 51% yield over two steps) as a yellow

color TFA salt: ^{1}H NMR (400 MHz, DMSO-d$_6$) δ 13.13 (br. s., 2H), 8.13 (br. s., 2H), 7.87 (t,

J=7.81 Hz, 1H), 7.59-7.67 (m, 2H), 7.50-7.59 (m, 3H), 5.73 (s, 2H); ^{19}F NMR (376 MHz,

DMSO-d$_6$) δ -73.77 (s, 3F, TFA), -108.59 (s, 1F); ^{13}C NMR (101 MHz, DMSO-d$_6$) δ 163.45 (t,

J$_{CF}$=7.63 Hz), 163.0 (d, [1]*J*$_{CF}$=244.64 Hz), 159.6 (q, *J*$_{CF}$=12.18 Hz), 154.1, 141.9, 135.4, 134.2,

126.4, 118.0, 116.3, 113.7 (d, *J*$_{CF}$=10.42 Hz), 112.8 (d, *J*$_{CF}$=27.48 Hz), 109.3 (d, *J*$_{CF}$=24.63 Hz),

109.0, 69.4; HRMS (ESI) m/z: calculated for $C_{16}H_{12}FN_5O$ [M + H]$^+$ 310.1099; observed

310.1107.

5-(((2-Methylpyridin-3-yl)oxy)methyl)quinazoline-2,4-diamine   dihydrochloride

(25a). To a solution of **41** (33.0 g, 136 mmol) in DMA (350 mL) was added guanidine carbonate

(49.1 g, 272 mmol). The reaction mixture was stirred at 140°C for 18 hours. The reaction mixture

was poured over ice, the precipitated solid was collected by filtration and washed with water,

dried *in vacuo* to afford 5-(((2-methylpyridin-3-yl)oxy)methyl)quinazoline-2,4-diamine (33.2 g,

86.6%) as yellow solid as free base. The solid was dissolved using water and conc. HCl, mixture

was lyophilized on the high vacuum to afford **25** (40.9 g, 98.4%) as a pink solid: LC/MS (ESI)

m/z 282.1 [M+H]$^+$; ^{1}H NMR (400 MHz, DMSO-d$_6$) δ 8.07 (d, *J*=4.68 Hz, 1H), 7.60 (d, *J*=8.20

Hz, 1H), 7.45 (d, *J*=7.81 Hz, 1H), 7.20-7.30 (m, 2H), 7.17 (d, *J*=7.02 Hz, 1H), 6.78 (br. s., 2H),

6.08 (br. s., 2H), 5.45 (s, 2H), 2.36 (s, 3H); ^{13}C NMR (101 MHz, DMSO-d$_6$) δ162.4, 160.0,

154.9, 151.4, 147.8, 141.1, 131.9, 131.6, 126.2, 123.9, 122.1, 119.4, 110.1, 69.6, 19.3; HRMS

(ESI) m/z: calculated for $C_{15}H_{15}N_5O$ [M + H]$^+$ 282.1349; observed 282.1351.

5-((1-(2,6-Dichlorobenzyl)piperidin-4-yl)methoxy)-7-methylquinazoline-2,4-diamine

(26). To a solution of **46** (150 mg, 0.522 mmol) and triethylamine (106 mg, 1.04 mmol) in DMF

(2 mL) was added **47** (138 mg, 0.574 mmol), the reaction stirred at 60 °C for 16 h. The solution

was poured over ice-water and precipitated solid was collected by filtration to afford **26** (130 mg,

55.8 %) as an off white solid: LC/MS (ESI) m/z 445.9 [M+H]$^+$; ^{1}H NMR (400 MHz, DMSO-d$_6$)

δ 7.47 (d, *J*=8.03 Hz, 2H), 7.34 (t, *J*=8.03 Hz, 1H), 7.12 (br. s., 2H), 6.60 (s, 1H), 6.39 (s, 1H),

5.93 (br. s., 2H), 3.96 (d, *J*=6.53 Hz, 2H), 3.69 (s, 2H), 2.78-2.96 (m, 2H), 2.28 (s, 3H), 2.22 (t,

J=10.79 Hz, 3H), 1.75 (d, *J*=12.05 Hz, 2H), 1.13-1.35 (m, 2H); ^{13}C NMR (101 MHz, DMSO-d$_6$)

δ 162.6, 162.5, 157.2, 156.4, 146.7, 136.6, 134.4, 130.3, 129.1, 111.2, 107.3, 98.5, 74.1, 56.8,

53.1, 35.1, 29.0, 22.3; HRMS m/z calcd for $C_{22}H_{25}Cl_2N_5O$ [M+H]$^+$: 446.1509. Found: 446.1508

5-((1-(2-Fluorobenzyl)piperidin-4-yl)methoxy)-7-methylquinazoline-2,4-diamine

(27). Compound **27** was prepared similarly to **26** using commercially available 1-(bromomethyl)-

2-fluorobenzene and 7-methyl-5-(piperidin-4-ylmethoxy)quinazoline-2,4-diamine **(46)** as

reagents in the nucleophilic displacement step: LC/MS (ESI) m/z 396.1 [M+H]$^+$; ^{1}H NMR (400

MHz, DMSO-d$_6$) δ 7.42 (t, *J*=6.78 Hz, 1H), 7.28-7.37 (m, 1H), 7.07-7.23 (m, 4H), 6.61 (s, 1H),

6.39 (s, 1H), 5.93 (br. s., 2H), 3.98 (d, *J*=6.02 Hz, 2H), 3.36 (s, 2H), 2.88 (d, *J*=11.04 Hz, 2H),

2.29 (s, 3H), 2.03 (t, *J*=10.79 Hz, 2H), 1.86 (br. s., 1H), 1.76 (d, *J*=12.05 Hz, 2H), 1.28-1.44 (m,

2H); ^{13}C NMR (101 MHz, DMSO-d$_6$) □ 162.5 (d, $^1J_{CF}$=247.51 Hz), 162.1, 161.2, 156.9, 155.6,

143.0, 132.0 (d, $^3J_{CF}$=5.03 Hz), 129.4 (d, $^3J_{CF}$=8.32 Hz), 125.2 (d, $^2J_{CF}$=14.77 Hz), 124.6 (d,

$^4J_{CF}$=3.5 Hz),, 117.2, 115.5 (d, $^2J_{CF}$=23.96 Hz), 103.8, 99.7, 73.5, 55.3, 53.0, 35.6, 29.2, 22.3; ^{19}F

NMR (376 MHz, DMSO-d$_6$) δ -118.10 (s, 1F); HRMS m/z calcd for $C_{22}H_{26}FN_5O$ [M+H]$^+$:

396.2194. Found: 396.2201.

3-((2,4-Diamino-7-methylquinazolin-5-yl)methoxy)-5-fluorobenzonitrile (28). To a

solution of **55** (1.47 g, 5.171 mmol) in DMA (16 mL) was added guanidine carbonate (1.86 g,

10.3 mmol) at 10°C. The reaction mixture was heated at 140 ^{o}C for 4 h, quenched by pouring

over ice-water and resulting solid filtered and washed with water. The residue was purified by

chromatography over silica gel eluting with gradient of DCM and MeOH (1:0 to 10:1) to give

the crude **28** (560 mg) as a brown solid. The solid was recrystallized from EtOH, dried on high

vacuum to give **28** (296 mg, 18%) as a light brown solid: LC/MS (ESI) m/z 323.9 [M+H]$^+$; ^{1}H

NMR (400 MHz, CD$_3$OD) δ 7.41 (s, 1H), 7.29-7.35 (m, 1H), 7.25 (d, *J*=8.03 Hz, 1H), 7.19 (s,

1H), 7.13 (s, 1H), 5.45 (s, 2H), 2.42 (s, 3H); ^{13}C NMR (101 MHz, DMSO-d$_6$) δ 163.0 (d,

$^1J_{CF}$=245.88 Hz), 162.6, 160.6, 159.6 (d, J_{CF}=12.93 Hz), 155.7, 141.9, 131.6, 126.0 (d, J_{CF}=26.67

Hz), 118.0 (d, J_{CF}=5.49 Hz), 116.3, 113.7 (d, J_{CF}=12.98 Hz), 112.8 (d, J_{CF}=25.46 Hz), 109.3 (d,

J_{CF}=24.46 Hz), 108.4, 71.0. 21.6; ^{19}F NMR (376 MHz, DMSO-*d$_6$*) δ ppm -108.5 (s, 1 F); HRMS

m/z calcd for C$_{17}$H$_{14}$N$_5$O [M+H]$^+$: 324.1255. Found: 324.1261.

7-Methyl-5-((tetrahydro-2H-pyran-4-yl)methoxy)quinazoline-2,4-diamine   **(29).**

Compound **29** was prepared similarly to **26** using commercially available (tetrahydro-2H-pyran-

4-yl)methanol and 2,6-difluoro-4-methylbenzonitrile **(43)** as reagents in the nucleophilic

displacement step followed by cyclization: LC/MS (ESI) m/z 289.2 [M+H]$^+$; ^{1}H NMR (400

MHz, CD$_3$OD) δ 6.74 (s, 1H), 6.54 (s, 1H), 3.93-4.14 (m, 4H), 3.52 (t, *J*=11.04 Hz, 2H), 2.39 (s,

3H), 2.12-2.31 (m, 1H), 1.81 (d, *J*=13.05 Hz, 2H), 1.52 (dq, *J*=4.52, 12.38 Hz, 2H); ^{13}C NMR

(101 MHz, DMSO-*d$_6$*) δ 162.07, 161.25, 156.84, 155.62, 142.97, 117.18, 103.84, 99.73, 73.52,

67.03, 34.65, 29.79, 22.31; HRMS m/z calcd for C$_{15}$H$_{20}$N$_4$O$_2$ [M+H]$^+$: 289.1659. Found: 289.167

2-Fluoro-6-((1-methoxypropan-2-yl)oxy)benzonitrile (36). To a stirred suspension of

sodium hydride (0.8 g, 20 mmol) in THF (20 mL) was added **35** (0.9 g, 10 mmol) at 0°C and

reaction stirred at same temperature for 1h. A solution of 2,6-difluorobenzonitrile **31** (1.39 g, 10

mmol) in THF (25 mL) was added at 0°C and reaction mixture stirred for 12h at room

temperature. The reaction mixture was poured over crushed ice-water, and extracted with ethyl

acetate. The organic layer was washed with brine, dried over MgSO$_4$, filtered and concentrated

in vacuum. The residue was purified by silica gel flash chromatography eluting with a gradient

of petroleum ether and EtOAc (10: 1 to 3:1) to afford **36** (1.2 g, 60%) as an oil: ^{1}H NMR (400

MHz, CDCl$_3$) δ 7.40-7.57 (m, 1H), 6.86 (d, *J*=8.59 Hz, 1H), 6.78 (t, *J*=8.39 Hz, 1H), 4.54-4.75

(m, 1H), 3.66 (dd, *J*=6.44, 10.34 Hz, 1H), 3.57 (dd, *J*=4.29, 10.54 Hz, 1H), 3.44 (s, 3H), 1.39 (d,

J=6.24 Hz, 3H).

5-((1-Methoxypropan-2-yl)oxy)quinazoline-2,4-diamine (racemic) (37). A mixture of

36 (1.2 g, 6 mmol) and guanidine carbonate (2.16 g, 12 mmol) in DMA (12 mL) was heated at

140°C for 12 h. The reaction mixture was cooled to room temperature and crude product was

purified by reverse phase HPLC using a gradient of water and acetonitrile (95:5 to 5:95) to give

racemic **37** (140 mg, 10 %) as a white solid: LC/MS (ESI) m/z 249.0 [M+H]$^+$.

2-(Bromomethyl)-6-fluorobenzonitrile (39). To a mixture of **38** (45.0 g, 333 mmol) and

NBS (53.3 g, 300 mmol) in carbon tetrachloride (450 mL) was added AIBN (2.73 g, 16.6 mmol).

The reaction was heated at reflux for 18 h, allowed to cool at room temperature and quenched

with saturated sodium thiosulfate. The reaction was extracted with DCM; organic layer was dried

over sodium sulfate, filtered and concentrated *in vacuo*. The residue was purified by silica gel

flash chromatography eluting with a gradient of petroleum ether and ethyl acetate (10: 0 to 2:8)

to afford **39** (42.5 g, 59.6%) as a white solid. ^{1}H NMR (400 MHz, CDCl$_3$) δ ppm 7.62 (m, 1H),

7.36 (d, *J*=6.2 Hz, 1 H), 7.17 (t, *J*=8.20 Hz, 1 H) 4.63 (2, 2H)

2-Fluoro-6-(((2-methylpyridin-3-yl)oxy)methyl)benzonitrile (41). To a mixture of **39**

(42.2 g, 197 mmol) and potassium carbonate (68.1 g, 493 mmol) in acetonitrile (400 mL) was

added **40** (21.5 g, 197 mmol). The mixture was stirred at room temperature for 18h, filtered and

the filter cake was washed with ethyl acetate (300 mL). The residue was purified by silica gel

flash chromatography eluting with a gradient of petroleum ether and ethyl acetate (5:1 to 3:1) to

afford **41** (33.0 g, 69.1%) as a yellow solid. ^{1}H NMR (400 MHz, CDCl$_3$) δ ppm 8.18 (d, *J*=6.2 Hz, 1H), 7.65 (m, 1H), 7.5 (d, *J*=7.80 Hz, 1 H), 7.23 (t, *J*=8.2 Hz, 1H), 7.22-7.07 (m, 2H), 5.26 (s, 2H), 2.57 (s, 2H)

2,6-Difluoro-4-methylbenzonitrile (43). To a solution of **42** (1 g, 4.59 mmol) in dioxane/water (5:1, 12 mL, degassed) was added methylboronic acid (412 mg, 6.88 mmol), tetrakis(triphenylphosphine)palladium(0) (530 mg, 0.459 mmol) and potassium carbonate (1.9 g, 14 mmol). The mixture was stirred at 110°C for 3 h under nitrogen. The suspension was concentrated *in vacuo* and residue was purified by silica gel flash chromatography eluting with a gradient of petroleum ether and ethyl acetate (10:1 to 3:1) to give **43** (0.37 g, 52.7%) as a white solid: ^{1}H NMR (400 MHz, CDCl$_3$) δ 6.87 (d, *J*=8.53 Hz, 2H), 2.45 (s, 3H).

t-Butyl 4-((2-cyano-3-fluoro-5-methylphenoxy)methyl)piperidine-1-carboxylate (44). A solution of **30** (0.50 g, 2.35 mmol) in DMF (5 mL) was added dropwise to a suspension of sodium hydride (0.141 g, 3.53 mmol, 60% in mineral oil) in DMF (2.5 mL) at 0 °C, reaction gradually warmed up to room temperature and stirred for 1 h. A solution of **43** (360 mg, 2.35 mmol) in DMF (2.5 mL) was cooled to 0 °C, and the alcohol mixture was added dropwise to the benzonitrile solution and stirred for 3 h. The solution was poured over ice-water. The precipitated solid was collected by filtration and residue was purified by silica gel flash chromatography using petroleum ether and ethyl acetate (1:1) to give **44** (0.3 g, 36.6%) as a colourless oil: LC/MS (ESI) m/z 371.2 [M+Na]; ^{1}H NMR (400 MHz, CDCl$_3$) δ 6.60 (d, *J*=9.03 Hz, 1H), 6.53 (s, 1H), 4.18 (br. s., 2H), 3.89 (br. s., 2H), 2.76 (br. s., 2H), 2.39 (s, 3H), 2.05 (br. s., 1H), 1.87 (d, *J*=12.05 Hz, 2H), 1.47 (s, 9H), 1.26 (dd, *J*=4.02, 12.05 Hz, 2H)

t-Butyl-4-(((2,4-diamino-7-methylquinazolin-5-yl)oxy)methyl)piperidine-1-carboxylate (45). A mixture of **44** (0.295 g, 0.847 mmol) and guanidine carbonate salt (0.305 g, 1.69 mmol) in DMA (5 mL) was heated at 140°C for 18 h. The solution was poured over ice-water. The precipitated solid was collected by filtration to afford **45** (0.25 g, 76.2 %) as a white solid: LC/MS (ESI) m/z 387.9 [M+H]$^{+}$; ^{1}H NMR (400 MHz, DMSO-d$_6$) δ 7.09 (br. s., 2H), 6.60 (s, 1H), 6.40 (s, 1H), 5.91 (br. s., 2H), 3.99 (m, 4H), 2.79 (m, 2H), 2.29 (s, 3H), 2.07 (m, 1H), 1.76 (d, J=12.05 Hz, 2H), 1.41 (s, 9H), 1.06-1.31 (m, 2H)

7-Methyl-5-(piperidin-4-ylmethoxy)quinazoline-2,4-diamine (46). A solution of HCl in dioxane (4M, 8 mL) was added to a solution of **45** (0.250 g, 0.645 mmol) in MeOH (8 mL). The solution was stirred at room temperature for 3 h under nitrogen. The precipitate was collected by filtration to afford **46** (0.165 g, 89 %) as a yellow solid; LC/MS (ESI) m/z 287.6 [M+H]$^{+}$; ^{1}H NMR (400 MHz, CD$_3$OD) δ 6.93 (s, 1H), 6.84 (s, 1H), 4.25 (d, J=6.53 Hz, 2H), 3.50 (d, J=12.55 Hz, 2H), 3.03-3.19 (m, 2H), 2.49 (s, 3H), 2.35-2.45 (m, 1H), 2.13 (d, J=13.55 Hz, 2H), 1.53-1.76 (m, 2H)

2-Bromo-6-fluoro-4-methylaniline (49). To a solution of **48** (30 g, 240 mmol) in acetic acid (240 mL) was added NBS (48 g, 270 mmol) in portions over 30 minutes at room temperature. The reaction turned from brown to red in color and was stirred for another 90 min. Water was added, and the mixture extracted into ethyl acetate (2 times). The combined organics were washed sequentially with 10% aqueous sodium carbonate, brine, dried over sodium sulfate, filtered and evaporated in vacuum. The residue was purified by column chromatography over silica gel which was eluted using a gradient of petroleum ether and ethyl acetate (1:0 to 3:1) to give **49** (28.4 g, 58%) as brown oil, which solidified on standing. ^{1}H NMR (400 MHz, CDCl$_3$) δ 7.03 (s, 1H), 6.78 (d, J=11.54 Hz, 1H), 3.96 (br. s., 2H), 2.23 (s, 3H)

2-Bromo-6-fluoro-4-methylbenzonitrile (50). Compound **49** (5 g, 20.0 mmol) was suspended in a mixture of water (10.5 mL) and glacial AcOH (17.5 mL) at 20 ^{o}C, concentrated H$_2$SO$_4$ (3.7 mL) was added dropwise at the same temperature. The mixture was cooled to 0 ^{o}C and a solution of sodium nitrite (2.0 g, 28.99 mmol) in water (3.7 mL) was added dropwise with vigorous stirring. In another 500 mL round-bottomed flask, copper(II) sulfate pentahydrate (7.65 g, 30.6 mmol) was dissolved in water (20 mL), and solution of KCN (8.0 g, 122.9 mol) in water (20 mL) was added dropwise slowly at 20 ^{o}C. NaHCO$_3$ (17.5 g, 208.32 mmol) and toluene (20 mL) were added and the reaction was placed in an oil bath preheated to 55 ^{o}C. To this flask, the above prepared solution of the diazonium salt was added dropwise with vigorous stirring over 30 minutes and heating continued for additional 30 min. The reaction was basified with NaOH (pH=11). The reaction was diluted with DCM, filtered over celite, organics extracted and washed with water and brine, dried over Na$_2$SO$_4$, filtered and evaporated in vacuum. The residue was purified by chromatography over silica gel eluting with gradient of petroleum ether and ethyl acetate (1:0 to 3:1) to give **50** (2.3 g, 40%) as a light brown solid. ^{1}H NMR (400 MHz, CDCl$_3$) δ 7.33 (s, 1H), 7.00 (d, *J*=9.03 Hz, 1H), 2.43 (s, 3H)

2-Fluoro-6-formyl-4-methylbenzonitrile (51). To a solution of **50** (2.2 g, 10 mmol) in THF (15 mL) was added i-PrMgCl (6.2 mL, 2M) drop wise at -40 ^{o}C, reaction continued for additional 3 h while maintaining internal temperature between -40 ^{o}C to -30 ^{o}C. DMF (2.25 g, 30.8 mmol) was added drop wise over 20 min and reaction warmed to 20°C for 1 h. The reaction mixture was cooled to -10 ^{o}C, quenched with slow addition of 2M aqueous HCl (22 mL) over 20 min and stirring continued at -10 ^{o}C for 30 min. Ethyl acetate was added, organic layer extracted, washed with brine, dried over Na$_2$SO$_4$ and concentrated. The residue was purified by chromatography over silica gel eluting with gradient of petroleum ether and ethyl acetate (1:0 to

5:1) to give **51** (1.37 g, 82%) as a yellow solid: ^{1}H NMR (400 MHz, CDCl$_3$) δ 10.25 (s, 1H), 7.66 (s, 1H), 7.32 (d, J=9.03 Hz, 1H), 2.53 (s, 3H)

2-Fluoro-6-(hydroxymethyl)-4-methylbenzonitrile (52). To a solution of **51** (1.27 g, 7.784 mmol) in EtOAc (30 mL, dried over Na$_2$SO$_4$) was added NaBH(OAc)$_3$ (3.3 g, 15.6 mmol) in portions at 20 $^{\circ}$C, after stirring for 30 min, reaction was heated to 40 $^{\circ}$C for 2 h. The reaction mixture was cooled to 10 $^{\circ}$C and quenched with water, aqueous phase extracted with EtOAc (2 times), combined organic layers dried over Na$_2$SO$_4$, filtered and concentrated in vacuum. The residue was purified by chromatography over silica gel eluting with gradient of petroleum ether and EtOAc (10:1 to 1:1) to give **52** (1.1 g, 86%) as a yellow solid: ^{1}H NMR (400 MHz, CDCl$_3$) δ 7.25 (d, J=9.03 Hz, 1H), 6.95 (d, J=9.54 Hz, 1H), 4.87 (d, J=4.52 Hz, 2H), 2.44 (s, 3H)

2-(Bromomethyl)-6-fluoro-4-methylbenzonitrile (53). To a solution of compound **52** (24.4 g, 147.73 mmol) in DCM (500 mL) was added carbon tetrabromide (162 g, 488 mmol) and triphenylphosphine (58.1 g, 222 mmol) at 10 $^{\circ}$C. The reaction mixture was stirred at room temperature for 18 h. The reaction solution was concentrated in vacuum to give **53** (238 g crude, contained about 33.6 g product, 100%) as brown oil, which was used for the next step directly without further purification.

2-((3-Cyano-5-fluorophenoxy)methyl)-6-fluoro-4-methylbenzonitrile (55). To a solution of **54** (20.2 g, 147 mmol) in acetonitrile (400 mL) was added K$_2$CO$_3$ (61.1 g, 442 mmol) and **53** (238 g, crude, contained about 33.6 g product, 147.33 mmol) at 10 $^{\circ}$C. The light brown suspension was stirred at 10°C for 18 h. The reaction mixture was concentrated in vacuum to remove acetonitrile. The residue was diluted with water and extracted with DCM. The organic layer was dried over Na$_2$SO$_4$, filtered and the filtrate was concentrated in vacuum. The residue

was purified by chromatography over silica gel eluted using a gradient of petroleum ether and

EtOAc (10:1 to 3:1) to afford **55** (28.2 g, 67.6%) as a light brown solid: ^{1}H NMR (400 MHz,

CDCl$_3$) δ 7.23 (s, 1H), 7.02-7.12 (m, 3H), 6.98 (dd, *J*=2.26, 9.79 Hz, 1H), 5.20 (s, 2H), 2.42-2.53

(m, 3H)

Cellular accumulation assay: HEK293T cells or lymphoblasts were plated at 1 x 10^6

cells per well of a 6-well plate and incubated overnight before being treated for 2 h with either

Concanamycin A (100 nM) or Baflamycin (50 nM) or an equivalent concentration of DMSO as

control. Thereafter, either Chloroquine (100 nM), or one of the diaminoquinazoline compounds

(10 nM) or an equivalent DMSO as control were added to the cells and incubated for a further

2.5 h after which a fresh solution of drug or DMSO was applied for a further 2.5 h incubation.

The medium was aspirated; cells were washed with PBS, scraped from plates, suspended and

counted before being pelleted, the supernatant removed and the pellet solubilized in acetonitrile

for determination of compound concentration.

ASSOCIATED CONTENT

Supporting Information. The Supporting Information is available free of charge on the ACS

Publications website at DOI: 10.1021/acs.jmedchem.xxxxxxx.

Molecule formula strings (CSV)

AUTHOR INFORMATION

Corresponding Author

E-mail: ariamala.gopalsamy@pfizer.com. Phone: (617) 674-7075

Notes

ABBREVIATIONS USED

DcpS – mRNA Decapping Scavenger Enzyme; SMA – Spinal Muscular Atrophy; SMN1 and SMN2 – Survival Motor Neuron genes 1 and 2; LipE – Lipophilic Efficiency; ADME – Absorption, Distribution, Metabolism and Excretion; HLM – human Liver Microsome; AcOH – Acetic Acid; DCE – 1,2-dichloroethane; DCM – dichloromethane; DMF – *N,N*-dimethylformamide; DMAP – 4-dimethylamino pyridine; DMSO – dimethylsulfoxide; DMA – *N,N*-dimethylacetamide; EtOH – ethanol; EtOAc – ethyl acetate; NBS – N-bromosuccinimide; $MgSO_4$ – magnesium sulfate; $Na_2S_2O_4$ – sodium sulfate; THF – tetrahydrofuran; SFC – Super critical fluid chromatography

REFERENCES

1.   Nurputra, D. K.; Lai, P. S.; Harahap, N. I. F.; Morikawa, S.; Yamamoto, T.; Nishimura, N.; Kubo, Y.; Takeuchi, A.; Saito, T.; Takeshima, Y.; Tohyama, Y.; Tay, S. K. H.; Low, P. S.; Saito, K.; Nishio, H. Spinal muscular atrophy: From gene discovery to clinical trials. *Ann. Hum. Genet.* **2013,** *77*, 435-463.

2.   Monani, U. R.; De Vivo, D. C. Neurodegeneration in spinal muscular atrophy: From disease phenotype and animal models to therapeutic strategies and beyond. *Future Neurol.* **2014,** *9*, 49-65.

3.   Calder, A. N.; Androphy, E. J.; Hodgetts, K. J. Small molecules in development for the treatment of spinal muscular atrophy. *J. Med. Chem.* **2016,** *59*, 10067-10083.

4.   Cherry, J. J.; Kobayashi, D. T.; Lynes, M. M.; Naryshkin, N. N.; Tiziano, F. D.;

Zaworski, P. G.; Rubin, L. L.; Jarecki, J. Assays for the identification and prioritization of drug

candidates for spinal muscular atrophy. *Assay Drug Dev. Technol.* **2014,** *12*, 315-341.

5.   Thurmond, J.; Butchbach, M. E. R.; Palomo, M.; Pease, B.; Rao, M.; Bedell, L.; Keyvan,

M.; Pai, G.; Mishra, R.; Haraldsson, M.; Andresson, T.; Bragason, G.; Thosteinsdottir, M.;

Bjornsson, J. M.; Coovert, D. D.; Burghes, A. H. M.; Gurney, M. E.; Singh, J. Synthesis and

biological evaluation of novel 2,4-diaminoquinazoline derivatives as SMN2 promoter activators

for the potential treatment of spinal muscular atrophy. *J. Med. Chem.* **2008,** *51*, 449-469.

6.   Jarecki, J.; Chen, X.; Bernardino, A.; Coovert, D. D.; Whitney, M.; Burghes, A.; Stack,

J.; Pollok, B. A. Diverse small-molecule modulators of SMN expression found by high-

throughput compound screening: Early leads towards a therapeutic for spinal muscular atrophy.

Hum. Mol. Genet. **2005,** *14*, 2003-2018.

7.   Hett, E. C.; Kyne, R. E., Jr.; Gopalsamy, A.; Tones, M. A.; Xu, H.; Thio, G. L.; Nolan,

E.; Jones, L. H. Selectivity determination of a small molecule chemical probe using protein

microarray and affinity capture techniques. *ACS Comb. Sci.* **2016,** *18*, 611-615.

8.   Singh, J.; Salcius, M.; Liu, S.-W.; Staker, B. L.; Mishra, R.; Thurmond, J.; Michaud, G.;

Mattoon, D. R.; Printen, J.; Christensen, J.; Bjornsson, J. M.; Pollok, B. A.; Kiledjian, M.;

Stewart, L.; Jarecki, J.; Gurney, M. E. DcpS as a therapeutic target for spinal muscular atrophy.

ACS Chem. Biol. **2008,** *3*, 711-722.

9.   Gu, M.; Fabrega, C.; Liu, S.-W.; Liu, H.; Kiledjian, M.; Lima, C. D. Insights into the

structure, mechanism, and regulation of scavenger mRNA decapping activity. *Mol. Cell* **2004,**

14, 67-80.

10.   Liu, H.; Kiledjian, M. Decapping the message: A beginning or an end. *Biochem. Soc. Trans.* **2006,** *34*, 35-38.

11.   Milac, A. L.; Bojarska, E.; Wypijewska del Nogal, A. Decapping scavenger (DcpS) enzyme: Advances in its structure, activity and roles in the cap-dependent mRNA metabolism. *Biochim. Biophys. Acta, Gene Regul. Mech.* **2014,** *1839*, 452-462.

12.   Li, Y.; Kiledjian, M. Regulation of mRNA decapping. *Wiley Interdiscip. Rev.: RNA* **2010,** *1*, 253-265.

13.   Liu, H.; Rodgers, N. D.; Jiao, X.; Kiledjian, M. The scavenger mRNA decapping enzyme DcpS is a member of the HIT family of pyrophosphatases. *EMBO J.* **2002,** *21*, 4699-4708.

14.   Chen, N.; Walsh, M. A.; Liu, Y.; Parker, R.; Song, H. Crystal structures of human DcpS in ligand-free and m7GDP-bound forms suggest a dynamic mechanism for scavenger mrna decapping. *J. Mol. Biol.* **2005,** *347*, 707-718.

15.   Van Meerbeke, J. P.; Gibbs, R. M.; Plasterer, H. L.; Miao, W.; Feng, Z.; Lin, M.-Y.; Rucki, A. A.; Wee, C. D.; Xia, B.; Sharma, S.; Jacques, V.; Li, D. K.; Pellizzoni, L.; Rusche, J. R.; Ko, C.-P.; Sumner, C. J. The DcpS inhibitor RG3039 improves motor function in SMA mice. *Hum. Mol. Genet.* **2013,** *22*, 4074-4083.

16.   Gogliotti, R. G.; Cardona, H.; Singh, J.; Bail, S.; Emery, C.; Kuntz, N.; Jorgensen, M.; Durens, M.; Xia, B.; Barlow, C.; Heier, C. R.; Plasterer, H. L.; Jacques, V.; Kiledjian, M.; Jarecki, J.; Rusche, J.; DiDonato, C. J. The DcpS inhibitor RG3039 improves survival, function and motor unit pathologies in two SMA mouse models. *Hum. Mol. Genet.* **2013,** *22*, 4084-4101.

17.   Black, W. C.; Percival, M. D. The consequences of lysosomotropism on the design of selective cathepsin K inhibitors. *ChemBioChem* **2006,** *7*, 1525-1535.

18.   Wang, Y.; Gao, A.; Xu, X.; Dang, B.; You, W.; Li, H.; Yu, Z.; Chen, G. The

neuroprotection of lysosomotropic agents in experimental subarachnoid hemorrhage probably

involving the apoptosis pathway triggering by cathepsins via chelating intralysosomal iron. *Mol.

Neurobiol.* **2015,** *52*, 64-77.

19.   Ashoor, R.; Yafawi, R.; Jessen, B.; Lu, S. The contribution of lysosomotropism to

autophagy perturbation. *PLoS One* **2013,** *8*, e82481.

20.   Garcera, A.; Bahi, N.; Periyakaruppiah, A.; Arumugam, S.; Soler, R. M. Survival motor

neuron protein reduction deregulates autophagy in spinal cord motoneurons in vitro. *Cell Death

Dis.* **2013,** *4*, e686.

21.   Custer, S. K.; Androphy, E. J. Autophagy dysregulation in cell culture and animals

models of spinal muscular atrophy. *Mol. Cell. Neurosci.* **2014,** *61*, 133-140.

22.   Drose, S.; Altendorf, K. Bafilomycins and concanamycins as inhibitors of v-ATPases and

p-ATPases. *J. Exp. Biol.* **1997,** *200*, 1-8.

23.   Xu, H.; Gopalsamy, A.; Hett, E. C.; Salter, S.; Aulabaugh, A.; Kyne, R. E.; Pierce, B.;

Jones, L. H. Cellular thermal shift and clickable chemical probe assays for the determination of

drug-target engagement in live cells. *Org. Biomol. Chem.* **2016,** *14*, 6179-6183.

24.   Hett, E. C.; Xu, H.; Geoghegan, K. F.; Gopalsamy, A.; Kyne, R. E.; Menard, C. A.;

Narayanan, A.; Parikh, M. D.; Liu, S.; Roberts, L.; Robinson, R. P.; Tones, M. A.; Jones, L. H.

Rational targeting of active-site tyrosine residues using sulfonyl fluoride probes. *ACS Chem.

Biol.* **2015,** *10*, 1094-1098.

25.   Freeman-Cook, K. D.; Hoffman, R. L.; Johnson, T. W. Lipophilic efficiency: The most

important efficiency metric in medicinal chemistry. *Future Med. Chem.* **2013,** *5*, 113-115.

26.   Jones, L. H.; Summerhill, N. W.; Swain, N. A.; Mills, J. E. Aromatic chloride to nitrile transformation: Medicinal and synthetic chemistry. *MedChemComm* **2010,** *1*, 309-318.

27.   Meanwell, N. A. Synopsis of some recent tactical application of bioisosteres in drug design. *J. Med. Chem.* **2011,** *54*, 2529-2591.

28.   Cherry, J. J.; DiDonato, C. J.; Androphy, E. J.; Calo, A.; Potter, K.; Custer, S. K.; Du, S.; Foley, T. L.; Gopalsamy, A.; Reedich, E. J.; Gordo, S. M.; Gordon, W.; Hosea, N.; Jones, L. H.; Krizay, D. K.; LaRosa, G.; Li, H.; Mathur, S.; Menard, C. A.; Patel, P.; Ramos-Zayas, R.; Rietz, A.; Rong, H.; Zhang, B.; Tones, M. A. Characterization of the in vitro and in vivo effects of 2,4-diaminoquinazoline inhibitors of the decapping scavenger enzyme DcpS: Context-spcific modulation of SMN transcript levels. Manuscript submitted.

29.   Bunnage, M. E.; Gilbert, A. M.; Jones, L. H.; Hett, E. C. Know your target, know your molecule. *Nat. Chem. Biol.* **2015,** *11*, 368-372.

FIGURES AND TABLES

1
(RG-3039)

2

3
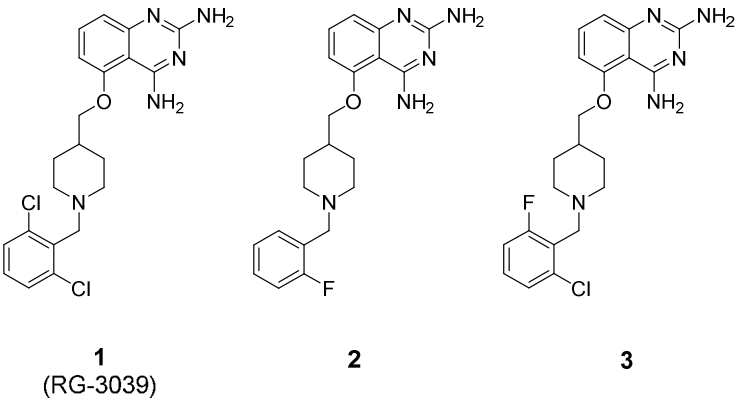
Figure 1. C5-substituted 2,4-diaminoquinazoline DcpS Inhibitors
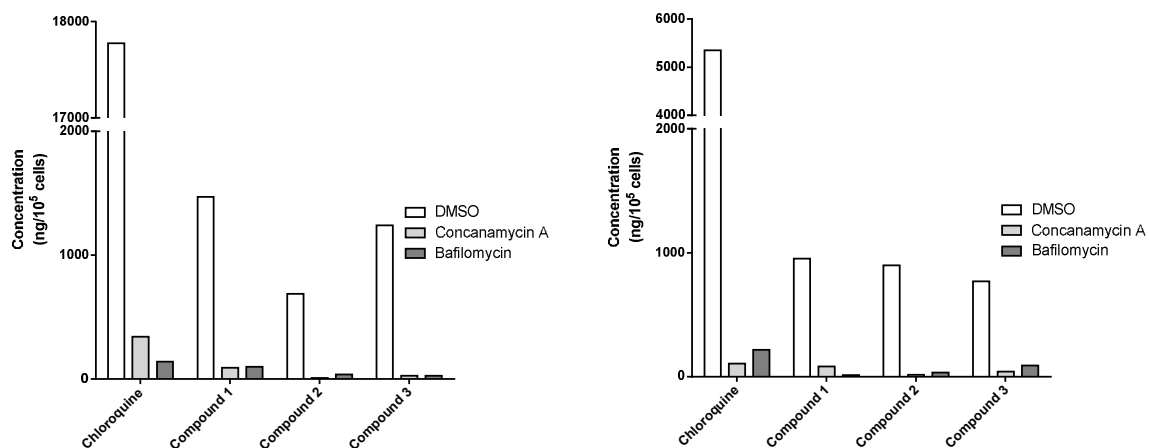
Figure 2. Concentration of DcpS inhibitors **1,2,3** and chloroquine (control) in the presence and absence of inhibitors of lysosomal acidification agents concanamycin-A and bafilomycin in HEK293T cells (Left panel) and lymphoblasts (Right panel).
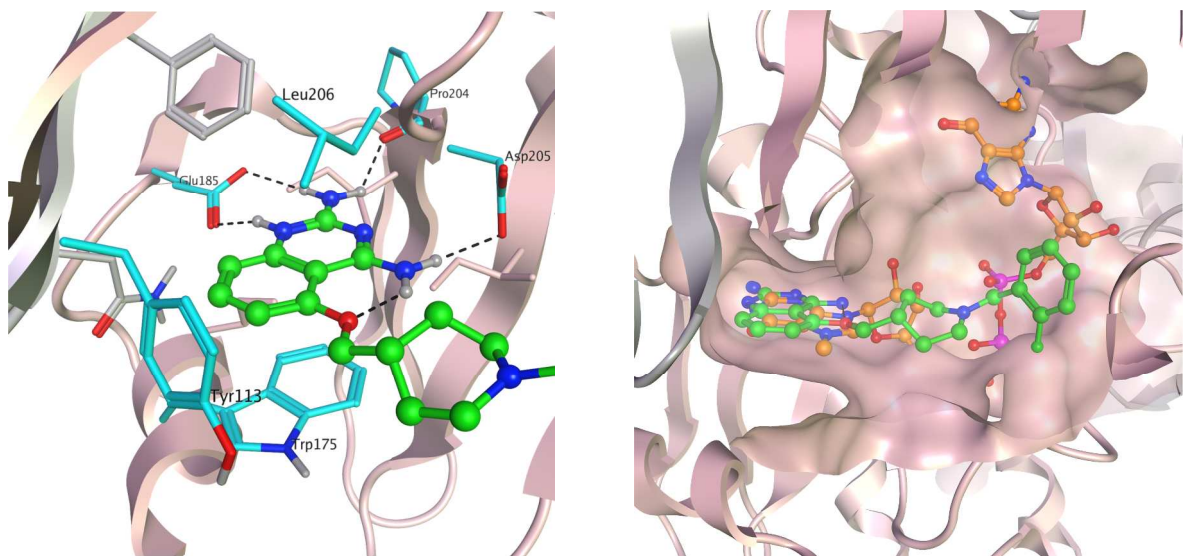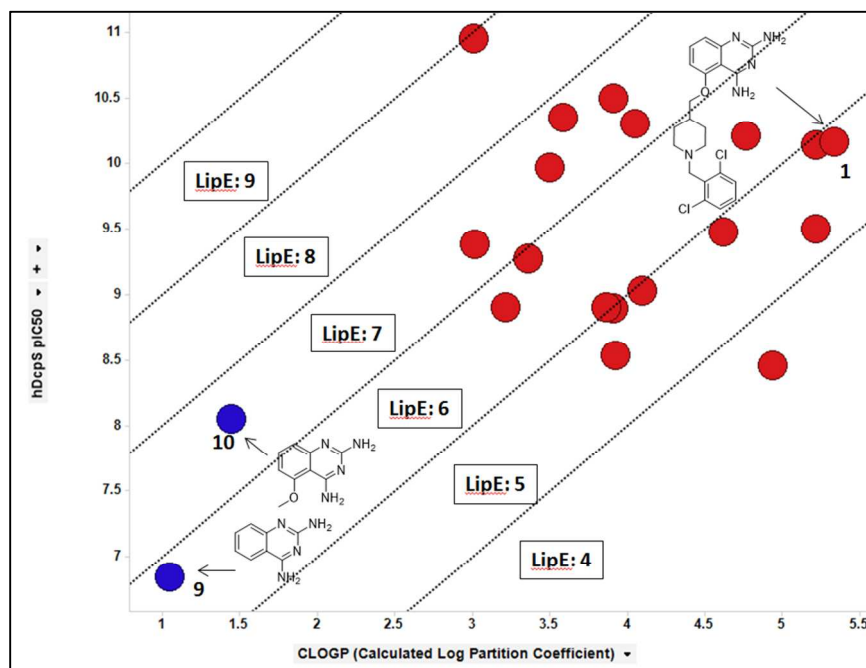
Figure 3. Left – Key interactions of Compound **2** (green) bound to DcpS. The interacting residues are shown in Cyan. Right – CAP (gold) bound in DcpS active site and overlay of Compound **2** (green) bound to DcpS.

A

B
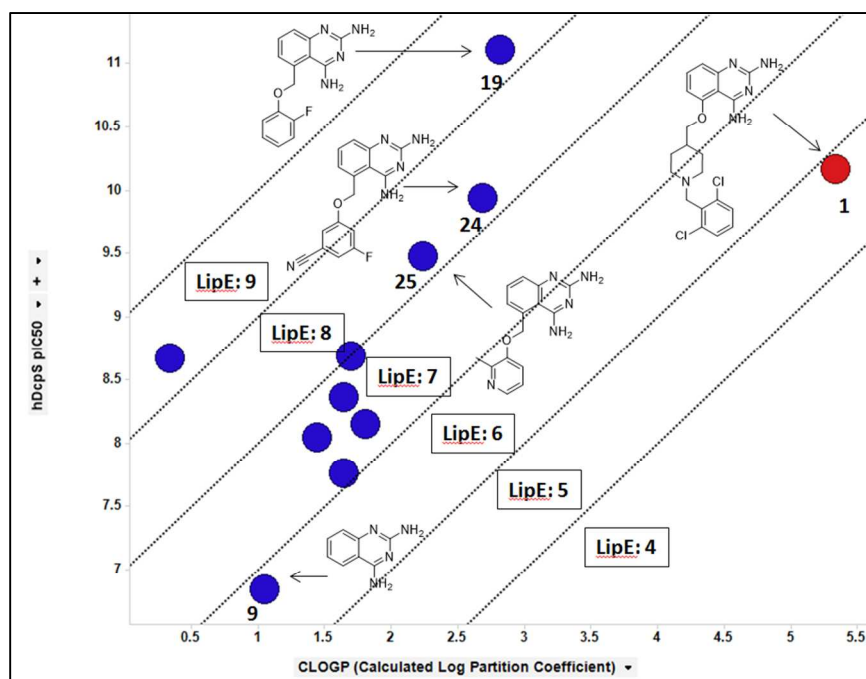
Figure 4. A. LipE plot of C-5 piperidinylmethoxy substituted 2,4-diaminoquinazolines in comparison to minimal pharmacophore (Compound **9** and **10**). B. LipE plot of C5-

aryl/hetaryloxymethyl substituted 2,4-diaminoquinazolines in comparison to RG-3039

(Compound **1**)
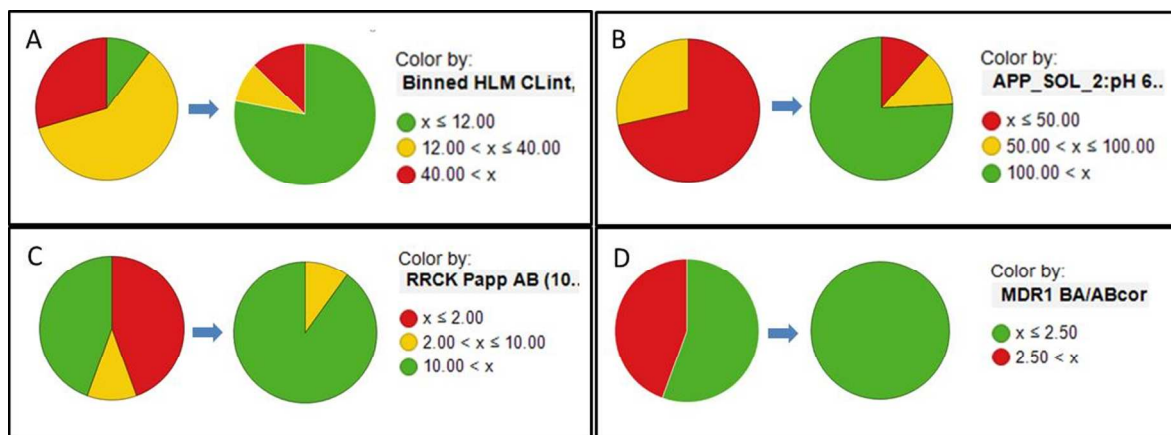
Figure 5. ADME properties comparison of piperidine analogs (left) vs non-piperidine analogs (right). A) measured HLM intrinsic clearance; B) measured apparent solubility (kinetic, uM); C) measured permeability; D) measured MDR (efflux).
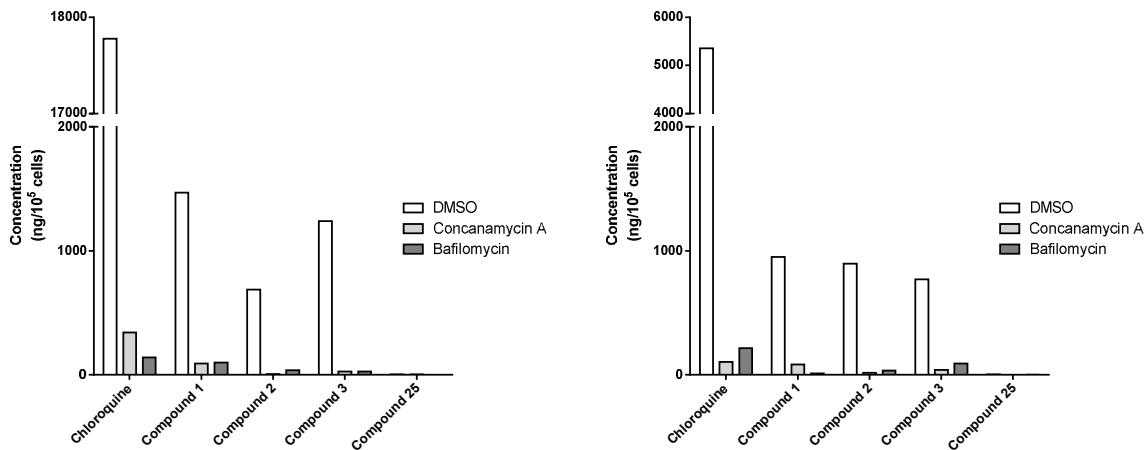
Figure 6. Concentration of DcpS inhibitors compound **1,2,3,25** and chloroquine (control) in the presence and absence of inhibitors of lysosomal acidification agents Concanamycin-A and Bafilomycin in HEK293T cells (Left panel) and lymphoblasts (Right panel).
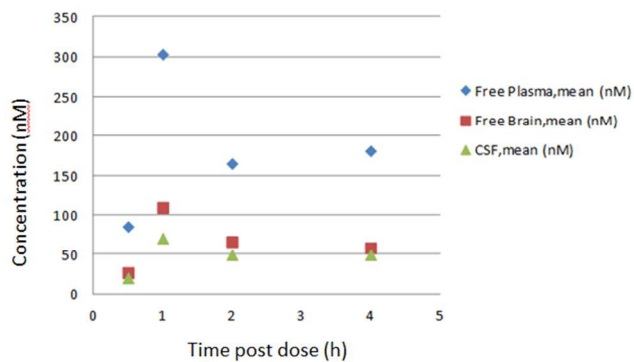
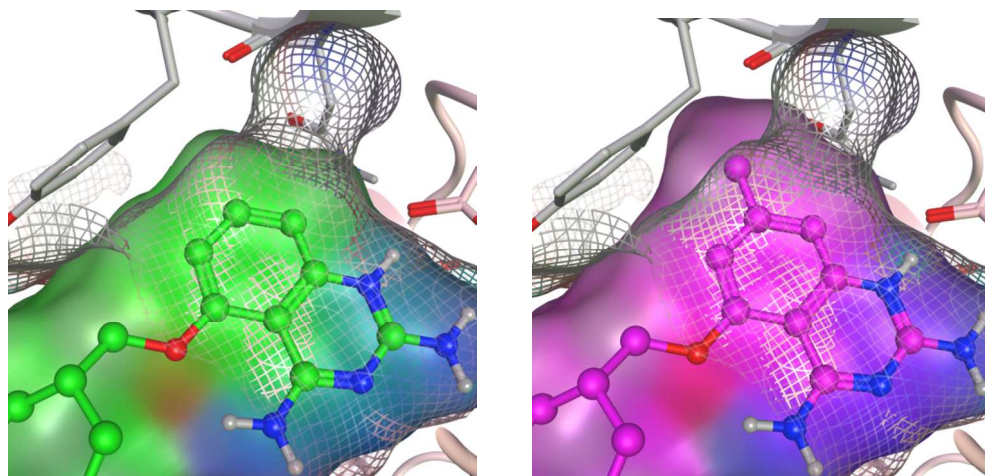**Figure 7.** Plasma, Brain and CSF PK of Compound **24** in FVB/N mice following 30 mg/Kg IP administration

Figure 8. Design of matched active-inactive pairs: Left: Compound **2** (green carbons) bound to

the cap binding pocket of DcpS. Connolly surface of the binding pocket (mesh representation)

highlights the compact fitting of the template (with molecular surface shown colored by ligand

atom) at the 7 position. Quinazoline template makes an edge to face interaction with Tyr 113.

Right: Shown is the 7-Methyl quinazoline template (magenta carbons, ligand surface colored by

ligand atom) which penetrates the binding pocket surface, with the methyl group resulting in a
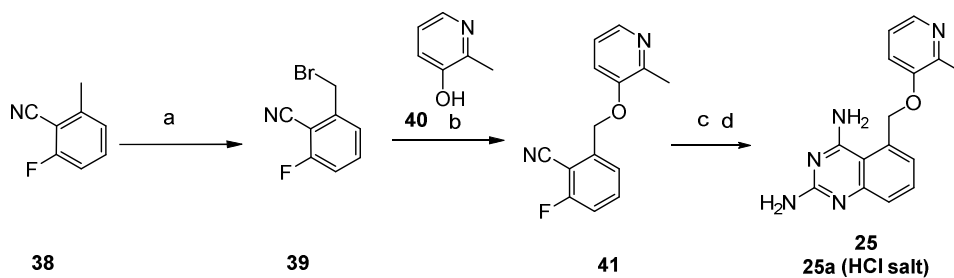
steric clash with Tyr 113.

Scheme 1. Synthesis of compounds **1-8**
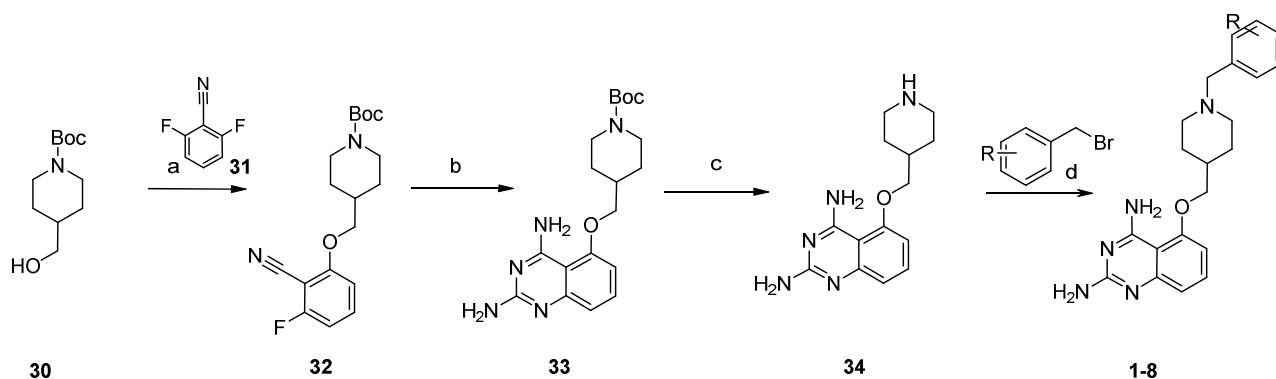
Reagents and conditions: (a) NaH, THF, 0°C to rt, 16h; (b) guanidine carbonate, DMA, 140°C, 8h; (c) HCl in methanol, rt, 4 h; (d) TEA, DMF, 70°C, 18 h

**Scheme 2.** Synthesis of alkyl ether compounds **15** and **16**
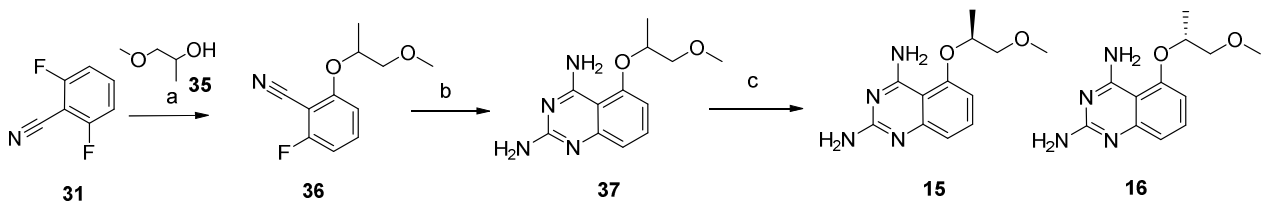
Reagents and conditions: (a) NaH, THF, 0°C to rt, 18h, 60%; (b) guanidine carbonate, DMA, 140°C, 12h, 10%; (c) chiral SFC (ChiralPak AD), 40% EtOH (0.05% NH₃ in H₂O), 80 mL/min, **15** (28%); **16** (28%).

1
2
3
4
5
6
7
8
9
10
11
12
13
14
15
16
17
18
19
20
21
22
23
24
25
26
27
28
29
30
31
32
33
34
35
36
37
38
39
40
41
42
43
44
45
46
47
48
49
50
51
52
53
54
55
56
57
58
59
60

Scheme 3. Synthesis of reverse ether compound **25**

38   39   41   25
                                    25a (HCl salt)

Reagents and conditions: (a) NBS, AIBN, carbontetrachloride, reflux, 18h, 60%; (b) K$_2$CO$_3$, MeCN, rt, 18h, 69%; (c) guanidine carbonate, DMA, 140°C, 18h, 87%; (d) conc. HCl, water, 98%

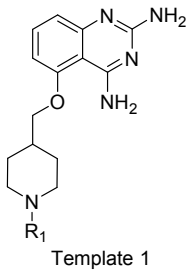**Scheme 4.** Synthesis of 7-methyl substituted ether compound **26**
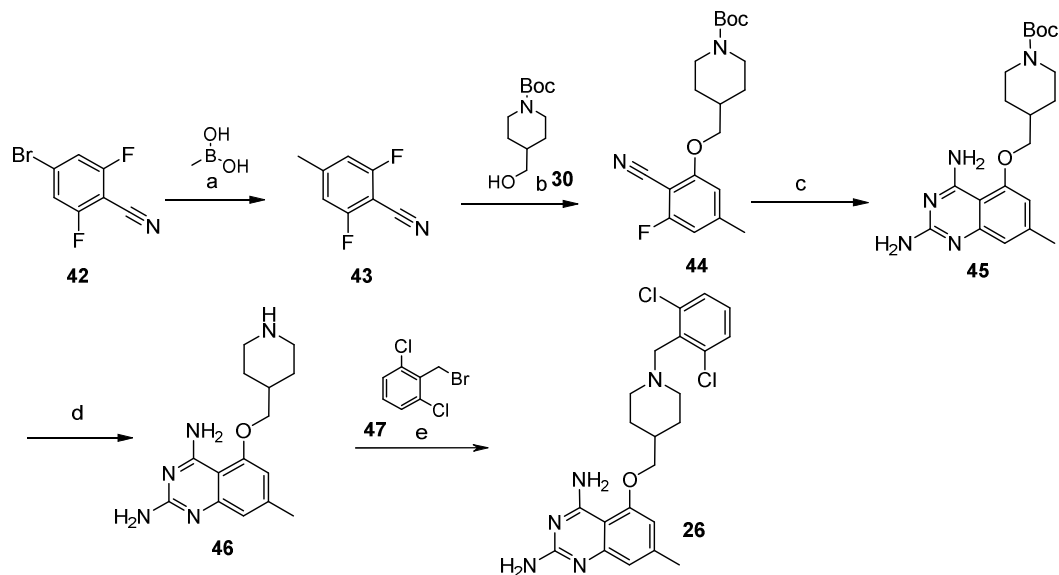
Reagents and conditions: (a) Pd(PPh$_3$)$_4$, K$_2$CO$_3$, Dioxane/H$_2$O, 110°C, 3 h, 53%; (b) NaH, DMF, 0°C to rt, 4h, 37%; (c) guanidine carbonate, DMA, 140°C, 18h, 76%; (d) HCl in methanol, rt, 3 h, 89%; (e) TEA, DMF, 60°C, 16 h, 56%

Scheme 5. Synthesis of 7-methyl substituted reverse ether compound **28**
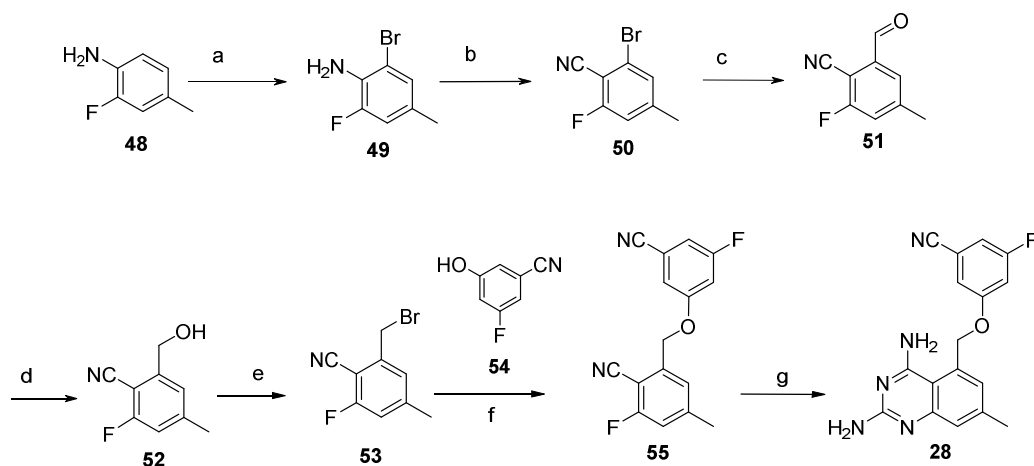
Reagents and conditions: (a) NBS, AcOH, rt, 58%; (b) AcOH-H$_2$O, NaNO$_2$, H$_2$SO$_4$, CuSO$_4$, KCN, 0$^{\rm o}$C to rt, 40%; (c) THF, iPrMgCl, DMF, -10$^{\rm o}$C to rt, 82%; (d) Na(OAc)$_3$BH, EtOAc, 20$^{\rm o}$C to 40$^{\rm o}$C, 2h, 86%; (e) CBr$_4$, PPh$_3$, DCM, 10$^{\rm o}$C to rt, quant. (f) K$_2$CO$_3$, MeCN, 10$^{\rm o}$C to rt, 18h, 67%, (g) guanidine carbonate, DMA, 140$^{\rm o}$C, 4h, 18%

**Table 1.** DcpS inhibition activity of C-5 substituted 2,4-diaminoquinazolines **1-8**[a]

Template 1

Compound	R1	DcpS Inhibition (nM)	cLogP	LipE
1	Cl / Cl (phenyl)	0.09	5.34	4.73
2	F (phenyl)	0.03	4.05	6.42
3	F / Cl (phenyl)	0.04	4.77	5.64
4	(phenyl)	0.03	3.91	6.59
5	OCF₃ (phenyl)	1.39	4.94	3.92
6	Cl (phenyl)	0.11	4.62	5.33
7	Cl / Cl (phenyl)	0.08	5.22	4.89

| 8 | | 0.32 | 5.22 | 4.28 |
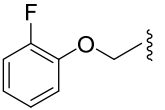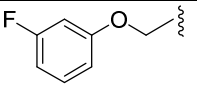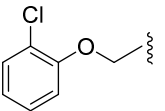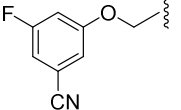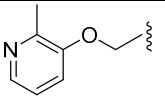
[a]All values are the mean of two or more independent assays.

Table 2. DcpS inhibition activity of C-5 substituted 2,4-diaminoquinazolines **9-25**[a]
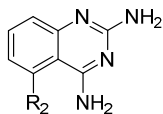
Template 2

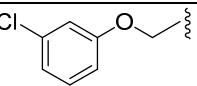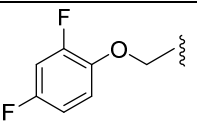| Compound	R2	DcpS Inhibition IC$_{50}$ (nM)	cLogP	LipE	DHFR IC$_{50}$ (μM)
9	H	142.58	1.05	5.80	ND
10		7.90	1.44	6.61	ND
11		1.01	3.21	5.69	ND
12		2.89[*]	3.93	4.62	ND
13		0.19	3.50	6.47	0.63
14		10.55	1.80	6.35	15
15		13.59	1.64	6.22	1.4
16		16.20	1.64	6.12	25
17		1.77	1.7	7.0	28
18		2.30	0.34	8.30	ND

19		0.02	2.82	8.29	>30
20		0.25	3.01	6.37	>50
21		0.29	3.36	5.92	ND
22		0.05	3.59	6.77	38
23		0.02	3.02	7.95	>50
24		0.11	2.69	7.28	52
25		0.27	2.24	7.33	>150

[a]All values are the mean of two or more independent assays. *Single determination. ND – Not determined

Table 3. *In-vitro* ADME and Physicochemical Properties of Analogs **1**, **24** and **25**

Compound	HLM app Clint, (μL/min/mg)[a]	RRCK Papp AB (10^{-6} cm/sec)[b]	MDR1 BA/AB[c]	Kinetic Solubility pH 6.5 (μM)	Measured LogD pH 7.4	MW	cLogP	TPSA
1	>250 (3 min)	0.62	>2.5	45	2.8	431	5.3	90
24	<8.4 (>115 min)	13	2.3	31	1.9	309	2.7	111
25	<8 (>120 min)	18	2.1	274	1.4	281	2.2	99

[a] – Human Liver Microsome stability – apparent intrinsic clearance (Dose: 1 μM)
[b] – RRCK assessment of permeability (RRCK2 cells were isolated from a culture of MDCK cells): Passive permeability Papp AB (Dose: 2 μM)
[c] – MDR1 assessment of P-glycoproteinefflux: MDCK/MDR1 permeability

1
2
3
4
5
6
7
8
9
10
11
12
13
14
15
16
17
18
19
20
21
22
23
24
25
26
27
28
29
30
31
32
33
34
35
36
37
38
39
40
41
42
43
44
45
46
47
48
49
50
51
52
53
54
55
56
57
58
59
60

Table 4. Compound **24** concentrations in FVB/N Mice

Compound **24**, 30 mpk, IP administration	
	Unbound C_{ave}
Plasma	173 nM
Brain	63 nM
CSF	47 nM

Table 5. DcpS activity of 7-H/7-Methyl matched pair C5-substituted 2,4-diaminoquinazolines[a]

7-H Analogs			7-Methyl Analogs		
Compound ID	Structure	DcpS IC$_{50}$ (nM)	Compound ID	Structure	DcpS IC$_{50}$ (nM)
1		0.069	**26**		334.3
2		0.049	**27**		12.31
24		0.115	**28**		>10000
17		2.1	**29**		>10000

[a]All values are the mean of two or more independent assays.

Table of Contents Graphic

1 (Cyan)
DcpS LipE: 4.73

24 (Purple)
DcpS LipE: 7.28